Development of a Portable 3D Ultrasound Imaging System for Musculoskeletal Tissues

Q.H. Huang[1], Y.P. Zheng[1], M.H. Lu[1] and Z.R. Chi[2]

1. Rehabilitation Engineering Center, The Hong Kong Polytechnic University, Kowloon, Hong Kong SAR, China

2. Centre for Multimedia Signal Processing and Communications
Department of Electronic and Information Engineering
The Hong Kong Polytechnic University,
Kowloon, Hong Kong SAR, China

Corresponding author:
Yongping Zheng, PhD.
Rehabilitation Engineering Center,
The Hong Kong Polytechnic University,
Hung Hom, Kowloon, Hong Kong SAR, P.R.China
Tel: 852-27667664
Fax: 852-23624365
Email: rczheng@inet.polyu.edu.hk

ABSTRACT

3D ultrasound is a promising imaging modality for clinical diagnosis and treatment monitoring. Its cost is relatively low in comparison with CT and MRI, no intensive training and radiation protection is required for its operation, and its hardware is movable and can potentially be portable. In this study, we developed a portable freehand 3D ultrasound imaging system for the assessment of musculoskeletal body parts. A portable ultrasound scanner was used to obtain real-time B-mode ultrasound images of musculoskeletal tissues and an electromagnetic spatial sensor was fixed on the ultrasound probe to acquire the position and orientation of the images. The images were digitized with a video digitization device and displayed with its orientation and position synchronized in real-time with the data obtained by a spatial sensor. A program was developed for volume reconstruction, visualization, segmentation and measurement using Visual C++ and Visualization toolkits (VTK) software. A 2D Gaussian filter and a Median filter were implemented to improve the quality of the B-scan images collected by the portable ultrasound scanner. An improved distance-weighted grid-mapping algorithm was proposed for volume reconstruction. Temporal calibrations were conducted to correct the delay between the collections of images and spatial data. Spatial calibrations were performed using a cross-wire phantom. The system accuracy was validated by one cylinder and two cuboid phantoms made of silicone. The average errors for distance measurement in three orthogonal directions in comparison with micrometer measurement were 0.06±0.39 mm, -0.27±0.27 mm, and 0.33±0.39 mm, respectively. The average error for volume measurement was -0.18%±5.44% for the three phantoms. The system has been successfully used to obtain the volume images of a fetus phantom, the fingers and

forearms of human subjects. For a typical volume with 126×103×109 voxels, the 3D image could be reconstructed from 258 B-scans (640×480 pixels) within one minute using a portable PC with Pentium IV 2.4 GHz CPU and 512 MB memories. It is believed that such a portable volume imaging system will have many applications in the assessment of musculoskeletal tissues because of its easy accessibility.

Keywords: 3D ultrasound imaging; free-hand scanning; musculoskeletal body parts; volume reconstruction

1. Introduction

Recently, growing attention in 3D diagnostic practice has led to a rapid progress of the development of 3D ultrasound equipment [1-3]. In comparison with CT and MRI imaging, 3D ultrasound is a low-cost solution for obtaining volume images. In addition, no intensive training and radiation protection is required for its operation, and its hardware is movable and can potentially be portable. Many different techniques have been recently developed for 3D ultrasound imaging. As acquisition approaches are concerned, they can be classified into four categories: 2-D transducer arrays, mechanical scanners, and freehand methods with and without positional information. The systems using 2-D transducer arrays can provide 3D images of a volume of interest in real-time, but they are expensive and not easily accessible yet. In the mechanical scanning methods, the ultrasound transducers are rotated or translated and the position data are obtained from the stepping motors in the scanning heads. Depending on the type of mechanical

motion, the acquired B-scans can be arranged in a sequence of parallel slices using linear motion [4], a wedge using tilt motion [5], a cone or a cylinder using rotational motion [6]. Mechanical scanning can normally provide high accuracy for the position measurement, but the range of motion is limited by the scanning device. Freehand scanning approaches allow clinicians to manipulate the ultrasound probe over the body surface with less constraint in comparison with mechanical scanning. The position and orientation of the probe can be recorded using position-sensing devices and used to reconstruct 3D data set. Some systems do not use any position-sensing device but estimate the relative positions and orientations between B-scans using the information derived from the images [7, 8]. However, this approach requires the probe to be moved smoothly in a single direction without significant rotation and translation between B-scans. In addition, this approach cannot provide an accurate distance or volume measurement due to errors caused by the estimation of movement during data acquisition.

The freehand techniques using position and orientation tracking device for spatial location have become more and more popular, as they offer free-hand operations for clinical applications [1, 2]. A typical freehand 3D ultrasound imaging system with position information normally comprises three primary parts: a 2D ultrasound scanner to acquire original 2D data, a 3D space locator to measure the position and orientation of the ultrasound probe, and a computer that contains corresponding software system to collect spatial data and 2D ultrasound images. The software is also used to reconstruct 3D data set, display 3D images, and analyse volume data. Various 3D spatial sensing approaches have been previously reported including electromagnetic position-sensing device [9-12], acoustic spark gaps [13], articulated arms [14], and optical sensors [15, 16]. Among all

reported methods, electromagnetic sensing is the most often used approach and portable devices are available. It uses a transmitter to generate a spatially varying magnetic field and a small spatial sensor attached to the ultrasound probe to sense the position and orientation. 2D B-scans and spatial position data are acquired simultaneously and later processed in the computer for volume reconstruction.

In the development of a free-hand 3D ultrasound imaging system, the essential objective is to reconstruct volume data using the collected B-scans and spatial information. The process of using the spatial information can be decomposed into three transformations between different coordinate systems as shown in Fig. 1. First, pixels on each B-scan are transformed from the coordinate system of the B-scan image plane *P* to the coordinate system of the electromagnetic receiver *R*. Then, pixels in *R* are transformed to the coordinate system of the electromagnetic transmitter *T* with respect to the measured data provided by the 3D space locator. Finally, pixels are transformed into the volume coordinate system *C* built up for volume reconstruction and visualization. Among the three transformations, the transformation from the image plane *P* to the receiver coordinate system *R* is unknown and therefore a calibration process must be implemented to find an accurate homogeneous matrix for this transformation. For a detailed discussion on this issue, the readers can refer to Prager et al. [17].

Another important processing step for the volume reconstruction of freehand 3D ultrasound imaging is the data interpolation, which is used to solve how the voxels of a 3D image are generated from the pixels of 2D images. A number of different methods have been previously reported [9, 10, 12, 18, 19]. Most of the approaches are simple and quick, as practical applications require real-time creation and the display of 3D free-hand

ultrasound data set. Those available methods can be mainly classified into voxel nearest-neighbour (VNN) interpolation [20], pixel nearest-neighbour (PNN) interpolation [21], and distance-weighted (DW) interpolation [9]. Besides these well-known methods, Rohling et al. [18] introduced an interpolation method based on radial basis function (RBF). Gaussian convolution kernel was also applied to reconstruct volume data [10, 12]. In addition, a Rayleigh interpolation algorithm was proposed by Sanches et al. [19] for improving the quality of reconstruction. These improved methods can provide better results of interpolation with a cost of increased computational complexity. Hence, most of them are not suitable for real-time clinical applications. In this study, we proposed a modified DW method to improve the trade-off between the interpolation accuracy and the computation time.

For clinical applications, musculoskeletal ultrasound has been proven to be a challenging area due to the complexity of various soft tissues and bones in musculoskeletal body parts [22]. It is difficult to obtain the spatial relationship between different tissues, such as bone, joint, tendon and muscles using 2D sonography. 3D ultrasound imaging can significantly improve the visualization of musculoskeletal disorders. Assessment of musculoskeletal tissues is commonly required in various fields including orthopaedics, physiotherapy and sports training, where on-site assessment is preferred.

Accordingly, this study was aimed to develop a portable 3D volumetric ultrasound imaging system for the assessment of 3D morphology of musculoskeletal tissues. The paper was organized as follows. In section 2, we described the development of our system using three separated portable devices for data collection and 3D image

reconstruction and display. In addition to the system design, an improved algorithm for volume reconstruction was introduced and experiments for evaluating our system were presented. In section 3, the experimental results of phantoms and human subjects were provided to demonstrate the performance of this system. Section 4 gave a discussion on this system and a conclusion was drawn in section 5.

2. Methods

2.1. System components

Our freehand 3D ultrasound system was comprised of three parts including a portable electromagnetic spatial sensing device, a portable ultrasound scanner, and a portable PC with software for data acquisition, 3D reconstruction and visualization (Fig. 2). The real-time position and orientation of the ultrasound probe in 3D space were recorded by the electromagnetic measurement system (MiniBird, Ascension Technology Corporation, Burlington, VT, USA). The spatial data including three translations (t_x, t_y, t_z) and an orientation matrix was transferred from the control box of MiniBird to the computer through its RS232 serial port. The sampling rate of MiniBird could be as high as 100 Hz so that sufficient data could be collected to improve the accuracy of the spatial information by averaging. The documented positional accuracy, positional resolution, angular accuracy, and angular resolution of MiniBird were 1.8 mm (RMS), 0.5 mm, 0.5° (RMS), and 0.1°, respectively, for a spherical range with a radius of 30.5 cm (MiniBird Manual, Ascension Technology Corporation, Burlington, VT, USA). We tested the positional accuracy of MiniBird at 10 cm using the 3D translating device and obtained an

average accuracy of -0.0602±0.208 mm. For the experiments described in the manuscript, the distance between the spatial sensor and the transmitter was kept as short as possible to achieve accurate results (in a range of approximately 10 cm to 20 cm). The receiver of MiniBird was mounted on the ultrasound probe of the portable real-time B-mode ultrasound scanner (SonoSite 180PLUS, SonoSite, Inc., Bothell, WA, USA). A linear probe (L38/10-5 MHz) was chosen to scan musculoskeletal body parts. A video capture card (NI-IMAQ PCI/PXI-1411, National Instruments Corporation, Austin, TX, USA) was installed in the PC and used to digitize real-time 2D ultrasound images. The maximum digitizing rate of the video capture card was 25 frames per second using the standard of PAL. In this system, 8-bit grey images were acquired by the video capture card. During data acquisition, spatial information and 2D digital ultrasound images were recorded simultaneously using software programmed in Visual C++. This software also provided functions for signal and image processing, volume reconstruction, visualization and analysis. Visualization toolkits (VTK, Kitware Inc., NY, USA) were integrated into the software for image processing and volume rendering. The software ran on the PC with 2.4 GHz Pentium IV microprocessor and 512 M bytes RAM.

2.2. Calibrations

Calibrations of the freehand 3D ultrasound imaging system included temporal calibration and spatial calibration [10, 20]. Since two independent devices were used to collect the spatial data and 2D B-scans, the delay between the two data streams during acquisition could not be avoided. Thus, temporal calibration was necessary to be performed for determining the temporal offset between time-stamps of the spatial

information and B-scans. Treece et al. [16] introduced a new method to conduct temporal calibration by comparing the difference between the positional data read from a spatial sensor attached on an ultrasound probe and those extracted from corresponding B-scans when the probe was manually moved towards the bottom of a water tank. In this paper, an improved temporal calibration approach was used to achieve more accurate results. We used a 3D translating device (Parker Hannifin Corporation, Irvine, CA, USA) to control the movement of the ultrasound probe so as to achieve steady movements of the probe. In addition, the probe movement direction could be controlled perpendicular to the bottom of the water tank to avoid the potential errors caused by the irregular probe movement in the case of manual manipulation. To avoid the possible influence from the metal parts of the translating device, the probe together with the electromagnetic sensor were hold by a plastic arm with a length of 0.5 m and its other end was fixed to the 3D translating device (Fig. 3). At the beginning of temporal calibration, the probe was submerged in the water tank, the bottom of which was shown as a horizontal line on the B-scan. After several seconds while the probe was kept steady, the probe was moved up and down at different rates by the 3D translating device and the line on the image went up and down accordingly. After approximately 22 seconds, the probe was kept steady again for one second. During the movement, all B-scans and spatial data were recorded. To get the temporal difference between the two data streams, we normalized the positions of lines shown on all B-scans and in those read from the spatial sensor both in the range of 0 to 1. The image sampling rate was set to 21 Hz, 16 Hz, 12 Hz, 9 Hz, and 5 Hz respectively while the maximum achievable sampling rate used for the spatial data collection ranged from 45 Hz to 100 Hz. For a comparison with the position data

extracted from the ultrasound images, the spatial data collected from the electromagnetic sensor were re-sampled to match each of the image sampling rates. Fig. 4(a) shows a typical temporal comparison between the normalized position data detected by the two systems with a sampling rate of 21 Hz. Time delays between the two sets of data can be obviously observed in Fig. 4(a). The exact time delay was obtained by shifting the position data obtained by the electromagnetic sensor from -50 ms to 50 ms with a step of 1 ms. For each step of shifting, the position data measured by the electromagnetic sensor were interpolated using a spline interpolation. The root-mean-square difference between the two sets of data was then calculated for each shift. Fig. 4(b) shows the root-mean-square differences calculated for the two data sets shown in Fig. 4(a). The time delay between the two sets of data corresponded to the temporal shift with the minimum root-mean-square difference.

The spatial calibration was performed to determine the spatial relationship between the B-scan image plane and spatial sensor attached on the probe. We conducted spatial calibration using a cross-wire phantom [23]. Two cotton wires were crossed in a water tank. The probe was moved at a speed of approximately 2 mm/s to scan over the crossing point. When a typical cross was displayed in the collected image, the image and the position and orientation data read from the spatial sensor were recorded. For each experiment, we captured 60 B-scans that displayed the cross from various directions and marked the centre of the cross manually. According to the position of each marker in the image plane and the position and orientation information read from spatial sensor, the three translation parameters (t_x, t_y, t_z) and three rotation parameters (α, β, γ) of the spatial

transformation from the B-scan plane to the coordinate system of the position sensor were calculated using a Levenberg-Marquardt nonlinear algorithm [17].

2.3. Scanning approach

Before data acquisition, the region to be scanned should be defined. Similar to the key frame method used by Barry et al. [9], we predefined two reference frames that determined the volume coordinate system *C* for volume reconstruction before data acquisition. As shown in Fig. 5, the two reference frames recorded before data acquisition represent the start position and end position of the region to be scanned. According to these two reference frames, the software created a cuboid volume with the width and height to be the same as those of a B-scan and the length to be the distance between the two upper-centre points of the two reference images. The z-axis of the volume was defined by calculating the vector from the start point to the end point as shown in Fig. 5. The x-axis and the y-axis of the volume were derived from the coordinates of the two reference B-scan planes recorded at the start position and the defined z-axis. Further corrections for x-axis, y-axis, and z-axis were conducted to make them a right-handed Cartesian coordinate system. The user could scan the probe within the defined region and all B-scans located inside the region would be used to reconstruct the volume. During scanning, the original B-scan image could be displayed with its position and orientation adjusted in real-time according to the collected spatial information (Fig. 6 (d)). The pre-defined volume could also be adaptively enlarged if the real scan region was beyond its boundary.

2.4. Data processing

Since the low cost portable ultrasound scanner had relatively poor image quality, different image processing methods including equalization, a 2D Gaussian filter ($\delta = 0.5$ to 2.0, kernel size = 3×3 pixels to 5×5 pixels) and a Median filter (3×3 pixels and 5×5 pixels) were used to improve the image quality. According to the needs of practical applications, the software provided functions for the operator to choose valid frames, to select region-of-interest (ROI), and to scale the size of ROI (Fig. 6). Defining ROI was to remove all description information like patient's name and experiment date. This function was realized by dragging the mouse to define a rectangle on an original B-scan and discarding the content outside the rectangle in all 2D B-scans. Properly reducing the size of frames and scaling ROI could make volume reconstruction easier and faster without compromising significantly the quality of the final reconstruction. In addition, a low-pass Gaussian filter was used to smooth the position and orientation data acquired by the electromagnetic spatial sensor.

2.5. Volume reconstruction

The volume reconstruction was divided into two stages, i.e. data mapping and gap filling. First, a volume coordinate system with a regular voxel array was defined in accordance with the scanning region and the size of ROI. In the stage of data mapping, each pixel from every B-scan was transformed to the volume coordinate system. Fig. 7 shows the 2D representation of this grid-mapping algorithm for volume reconstruction. For each voxel in the volume, we defined a sphere region centred about it. The weight of the contribution of each involved pixel was determined by the distance from the pixel to

the centre of the voxel. The final value of the voxel was the weighted sum of the intensities of all pixels falling in this sphere region. This process can be described as:

$$\vec{V}_C = M_{T\to C} M_{R\to T} M_{P\to R} \vec{V}_P \quad (1)$$

where $\vec{V}_P$ is the vector of a pixel in the coordinate system of image plane, $\vec{V}_C$ is the transformed vector of the pixel in the volume coordinate system, $M_{T\to C}$, $M_{R\to T}$ and $M_{P\to R}$ are three matrices transforming vectors from the image plane to the volume coordinates (Fig. 1).

If the size of a voxel was set larger than a pixel, it was possible that more than one pixel was transformed to the same grid of the voxel, while gaps might also result when no pixel fallen into some grids in the volume. To solve such a problem, Barry et al. [9] used a spherical region for each voxel and computed the weighted average of all pixels in this region using the inverse distance as the relative weight. However, if the range of the spherical region was set too large, the volume appeared being highly smoothed; otherwise gaps remained there [18].

In this study, we proposed a squared distance weighted (SDW) interpolation for the volume reconstruction. The algorithm can be described as follow:

$$I\left(\vec{V}_C\right) = \frac{\sum_{k=0}^{n} W_k I\left(\vec{V}_P{}^k\right)}{\sum_{k=0}^{n} W_k}; \qquad W_k = \frac{1}{\left(d_k + \alpha\right)^2} \quad (2)$$

where $I\left(\vec{V}_C\right)$ is the intensity of the voxel at the volume coordinate $\vec{V}_C$, n is the number of pixels falling within the pre-defined spherical region centred about voxel $\vec{V}_C$, $I\left(\vec{V}_P{}^k\right)$ is the intensity of the kth pixel at the kth image coordinate $\vec{V}_P{}^k$, W_k is the relative weight

for the *k*th pixel, d_k is the distance from the *k*th vector transformed from $\vec{V}_P{}^k$ to the centre of the voxel ($\vec{V}_C$), and α is a positive parameter for adjusting the effect of the interpolation. As SDW offered a non-linear assignment for the weights, the interpolated voxel array was expected to be less blurred in comparison with the DW method. Furthermore, it was expected that the decreased computation complexity could lead to a faster reconstruction in comparison with other non-linear methods such as using 3D Gaussian convolution kernel [10, 12]. The reconstructed images and computing times using DW, SDW, and 3D Gaussian convolution kernel methods were compared for a typical image set collected from a subject's finger.

If the spherical region for the interpolation was not large enough, some voxel grids could not be filled with pixels from the 2D image data. On the other hand, if the spherical region was too large, the image would be blurred and details could not be observed. To avoid the discontinuity of the intensity of voxels caused by empty grids, further interpolation should be performed to compute all empty grids in the gap-filling stage. A variety of methods had been reported for filling the gaps, including replacing a empty voxel with the nearest non-empty voxel, averaging of filled voxels in a local neighbourhood, bilinearly interpolating between two closest filled voxels in the transverse direction to the B-scans, and creating a 'thick' B-scan by convolving the 2D B-scan with a truncated 3D Gaussian kernel [18]. To produce an improved trade-off between the computation time and performance, a new algorithm of interpolation was implemented in this study. For each blank voxel, the radius of the spherical region centred about the voxel was enlarged to include more voxels for calculating the weighted average value using SDW. If the radius was large enough and exceeded a pre-set

threshold and there was still no value-assigned voxel within the enlarged region, the value of the blank voxel was set to zero. The locations of such voxels were recorded for the operator to judge whether the reconstructed volume was acceptable or not.

2.6. Volume visualization and analysis

The reconstructed volume was rendered with the Ray-casting algorithm [24]. The shading parameters could be adjusted by the user to achieve desired display of the volume. Functions of reslicing volume, clipping volume, and generating orthogonal slices were also provided for the analysis of the volume. Fig. 8 (a) shows a typical forearm volume which was clipped from different directions. A typical three orthogonal slices of the forearm volume is shown in Fig. 8 (b). The functions measuring distance, area, and volume were also implemented in the software.

2.7. Validation experiments

A cylindrical silicone phantom (diameter = 23.19 mm, height = 10.75 mm) and two cuboid silicone phantoms with sizes of 17.00×17.00×10.65 mm^3 and 10.56×10.45×14.64 mm^3 respectively were scanned and their volumes were reconstructed to assess the accuracy of the 3D ultrasound imaging system. These phantoms were fixed on the bottom of the water tank. As the propagation speed of ultrasound in silicone material is different from that in water, the bottom line of the silicone phantom shown in a B-scan was lower than the bottom of the water tank. According to the raw B-scan images, the distance between the surface and the bottom of a silicone phantom was approximately 1.5 times longer than that between the surface of

the phantom and the bottom of the water tank. According to our measurement, the mean speeds of sound in the silicone materials and in water at 22 °C were 958 m/s and 1491 m/s, respectively. We scaled the distance between the surface line and the bottom line of a silicon phantom by using a specially designed function in our program to manually mark the two lines and automatically elevate the bottom line of the phantom according to the ratio of the two ultrasound speeds in the collected images. Since the three silicone phantoms mentioned above were relatively small in comparison with adult human limb parts, the number of B-scans collected in a single sweep, which could fully cover a phantom, was no more than 80 in this study; hence the corrections for all B-scans could be made within 10 minutes. This semi-automatic correction was only used for the three silicone phantoms in this paper.

In this study, four sweeps of 2D images were collected from different directions and four corresponding volumes were reconstructed for each phantom. The differences between the phantom dimensions measured by a micrometer and those measured from the volumes were calculated. Similar calculations were conducted for the volumes measured by the two methods. In addition to those phantoms with regular shapes, a fetus phantom (Model 065-36, CIRS, Inc., Norfolk, VA, USA) was tested.

2.8. In-vivo experiments

To demonstrate its clinical applications, the 3D ultrasound system was used to scan the real musculoskeletal body parts of adult subjects (n = 3) *in vivo*. A water tank with a dimension of 40cm×40cm×15cm was used for containing the musculoskeletal body parts to be scanned. The water temperature for the experiments was approximately

23±1°C. During scanning, the body part was submerged in the water tank and kept steady. The probe was moved smoothly over the body parts to avoid obvious artefacts. In this study, both fingers and forearm were scanned.

3. Results

The experiments for the phantoms and the subjects demonstrated that the portable 3D ultrasound imaging system was reliable to obtain 3D volumes. For an image size of 640×480 pixels, the system could collect ultrasound images in a frame rate up to 21 frames per second. According to the requirements of different applications, the frame rate and image size could be adjusted by the operator. A typical volume of 126×103×109 voxels could be reconstructed from 258 B-scan images within one minute using the present system if the diameter of the spherical region for interpolation was not larger than 5 voxels.

According to the fifteen temporal calibration experiments, the mean temporal delay was 4.73 ms with a standard deviation of ±4.43 ms. The spatial calibration results including three translation and three rotation parameters are shown in Table 1. The results were calculated from 10 spatial calibration experiments using the cross-wire phantom.

The typical reconstructed 3D volumes of the cylindrical and cuboid phantoms are shown in Fig. 9(a) and Fig. 9(b), respectively. The dimensions and volumes of the phantoms measured by the micrometer and the 3D ultrasound imaging system are presented in Fig. 10 and Table 2. According to these measurement data, the overall average errors for the distance measurement in three orthogonal directions were

0.06±0.39 mm, -0.27±0.27 mm, and 0.33±0.39 mm, respectively. The average error for the volume measurement of the three phantoms tested was -0.18%±5.44%.

The right hand of the fetus phantom was scanned and the volume was reconstructed as shown in Fig. 9(c). Though the reconstructed surface was not as smooth as the real one, the hand and the fingers of the fetus could be observed clearly. Fig. 11(a) gives a 3D image for the fingers of the subject reconstructed from 493 B-scans. Fig. 11(b) shows a volume reconstructed from 297 B-scans for part of the forearm of the subject. A typical slice obtained from the reconstructed volume is shown in Fig. 11(c) and its corresponding B-scan image collected at the approximately same location is shown in Fig. 11(d). It can be obviously seen that the reconstructed slice and the original B-scan had almost identical image features.

To compare the results of different volume reconstruction methods, a subject's finger was scanned with 258 2D images (640×480 pixels) and its volume (205×175×273) was reconstructed using DW, SDW, and Gaussian convolution kernel algorithms. The diameter of the spherical region for interpolation was consistently set to 9 voxels for the implementation of the three algorithms. For the SDW method elaborated in Eq. (2), the parameter α was set to be 0.33. From the 2D images resliced from the same location of the volumes constructed using different methods, it could be seen that the DW algorithm significantly smoothed the image (Fig. 12(a) and (d)). The SDW and Gaussian kernel algorithms produced similar results (Fig. 12(b), (c), (e), and (f)). The computation times used by the DW, SDW, and Gaussian kernel methods were 161.5 s, 193.1 s, and 424.3 s, respectively in our system. The algorithm using the SDW method was 2.2 times faster than that using the Gaussian kernel method.

4. Discussion

A number of 3D freehand ultrasound systems have been previously introduced [9-12, 16]. However, all of them were not designed for portable use. In those systems, 2D ultrasound images were normally generated by high-quality ultrasonic devices and graphics workstations were used for accelerating volume reconstruction and visualization and for achieving high quality images. In comparison, we developed a portable 3D ultrasound imaging system using a relatively low-cost and portable ultrasound scanner, a portable 3D spatial locator, and a portable PC. It can be used in various clinical applications, where 3D images of subjects are preferred to take on-site. As demonstrated in this study, the portable 3D ultrasound system could reliably provide the volume images of the subject's fingers and forearms. We expected that the portable 3D ultrasound system would be particularly useful for the assessment of musculoskeletal body parts, such as physiotherapy, sports training, and on-site diagnosis of musculoskeletal tissue injuries. Currently, only ultrasound can provide 3D volume imaging with a portable setup.

For clinical applications, particularly for on-site imaging, real-time systems are highly required for fast diagnosis. Though computer hardware has been greatly improved recently, the long computation time (from a few minutes to a few hours [18]) required for the volume reconstruction still introduces many limitations for on-site applications of freehand 3D ultrasound imaging. The algorithms based on complicated mathematical models could provide good reconstruction results with a cost of computation time. For instance, Gaussian convolution kernel [10] is able to improve the quality of volume data,

but the exponential calculation in the Gaussian convolution operator makes the computation time of reconstruction longer in comparison with the conventional DW (the later one was 2.6 times faster using the present system). A more complicated algorithm described by Rohling et al. [18] could further improve the performance but required even more computing time (a few hours as reported by the authors) and leads to an inevitable disadvantage for on-site clinical applications. Giving attention to both the quality of volume and computing time, we proposed a new interpolation method, named as squared distance weighted, or SDW. It could be used to reconstruct the volume data with more details resolved in comparison with the conventional DW interpolation and a significantly reduced computation time (2.2 times faster using the present system) in comparison with the Gaussian convolution kernel method. However, the comparison for image quality was only conducted in a qualitative way in this study. Quantitative comparisons for the reconstruction results obtained using SDW and other methods are necessary to further demonstrate the advantage of this new method.

The dimensions and volumes of the phantoms measured by the portable 3D ultrasound system well agreed with those measured by the micrometer. The overall errors of the dimension and volume measurements were 0.02±0.43 mm and -0.18%±5.44%, respectively. In addition to further increasing the accuracy of the measurements and to further decreasing the computation time for volume reconstruction, we plan to use this system for the assessment of various musculoskeletal disorders. As demonstrated in this study, segmentation for different components of musculoskeletal tissues requires more efforts in comparison with that for fetus or internal organs.

5. Conclusions

We reported the development of a portable 3D free-hand ultrasound system in this paper. Validation results for the dimension and volume measurements were also reported together with preliminary volume images of the subject's fingers and forearms. In addition, we proposed a new algorithm for volume reconstruction based on square distance weighted interpolation. This algorithm could reduce the computation time by 2.2 times in comparison with the Gaussian convolution kernel method but could produce similar reconstruction quality. A typical volume with 126×103×109 voxels could be reconstructed from 258 B-scans (640×480 pixels) within one minute using a portable PC with Pentium IV 2.4 GHz CPU and 512 MB memories. The results presented in this paper have proved that our 3D free-hand ultrasound imaging system is very useful for the assessment of musculoskeletal body parts as well as other applications. We believe that the portability and easy accessibility can become unique features of 3D ultrasound imaging in comparison with CT and MRI. These features can greatly expand the applications of volume imaging beyond what currently can be obtained in the imaging department in the hospital.

Acknowledgements

This work was partially supported by the The Hong Kong Polytechnic University (G-YD42) and the Research Grants Council of Hong Kong (PolyU 5245/03E).

References

[1] T.R. Nelson, D.H. Pretorius, Three-dimensional ultrasound imaging, Ultrasound Med. Biol. 24(9) (1998) 1243-1270.

[2] A. Fenster, D. B. Downey, H. N. Cardinal, Three-dimensional ultrasound imaging, Phys. Med. Biol. 46(5) (2001) R67-R99.

[3] A. H. Gee, R. W. Prager, G. M. Treece, L. Berman, Engineering a freehand 3D ultrasound system, Pattern Recogn Lett. 24(4-5) (2003) 757-777.

[4] Z. Y. Guo, A. Fenster, Three-dimensional power Doppler imaging: A phantom study to quantify vessel stenosis, Ultrasound Med. Biol. 22(8) (1996) 1059-1069.

[5] D.B. Downey, D.A. Nicolle, M.F. Levin, A. Fenster, Three-dimensional ultrasound imaging of the eye, Eye 10 (1996) 75-81.

[6] P. He, Spatial compounding in 3D imaging of limbs, Ultrasonic Imaging 19(4) (1997) 251-265.

[7] T. A. Tuthill, J. F. Krucker, J. B. Fowlkes, P. L. Carson, Automated three-dimensional US frame positioning computed from elevational speckle decorrelation, Radiology 209(2) (1998) 575-582.

[8] R. W. Prager, A.H. Gee, G. M. Treece, C. J. C. Cash, L. Berman, Sensorless freehand 3-D ultrasound using regression of the echo intensity, Ultrasound Med. Biol. 29(3) (2003) 437-446.

[9] C. D. Barry, C. P. Allott, N. W. John, P. M. Mellor, P. A. Arundel, D. S. Thomson, J. C. Waterton, Three-dimensional freehand ultrasound: Image reconstruction and volume analysis, Ultrasound Med. Biol. 23(8) (1997) 1209-1224.

[10] S. Meairs, J. Beyer, M. Hennerici, Reconstruction and visualization of irregularly sampled three- and four-dimensional ultrasound data for cerebrovascular applications, Ultrasound Med. Biol. 26(2) (2000) 263-272.

[11] R. W. Prager, A. H. Gee, G. M. Treece, L. Berman, Freehand 3D ultrasound without voxels: volume measurement and visualisation using the Stradx system, Ultrasonics 40(1-8) (2002) 109-115.

[12] R. San José-Estérpar, M. Martín-Fernándes, P. P. Caballero-Martínes, C. Alberola-Lopes, J. Ruiz-Alzola, A theoretical framework to three-dimensional ultrasound reconstruction from irregularly sampled data, Ultrasound Med. Biol. 29(2) (2003) 255-269.

[13] D. L. King, D. L. King, M. Y. C. Shao, 3-Dimensional spatial registration and interactive display of position and orientation of real-time ultrasound images, J. Ultras. Med. 9(9) (1990) 525-532.

[14] E. A. Geiser, L. G. Christie, D. A. Conetta, C. R. Conti, G. S. Gossman, A mechanical arm for spatial registration of two-dimensional echocardiographic sections, Catheter and Cardio Diag. 8(1) (1982) 89-101.

[15] L. G. Bouchet, S. L. Meeks, G. Goodchild, F. J. Bova, J. M. Buatti, W. A. Friedman, Calibration of three-dimensional ultrasound images for image-guided radiation therapy, Phys. Med. Biol. 46(2) (2001) 559-577.

[16] G. M. Treece, A. H. Gee, R. W. Prager, C. J. C. Cash, L. Berman, High-definition freehand 3-D ultrasound, Ultrasound Med. Biol. 29(4) (2003) 529-546.

[17] R. W. Prager, R. N. Rohling, A. H. Gee, L. Berman, Rapid calibration of 3-D freehand ultrasound, Ultrasound Med. Biol. 24(6) (1998) 855-869.

[18] R. N. Rohling, A. H. Gee, L. Berman, A comparison of freehand three-dimensional ultrasound reconstruction techniques, Med. Image Anal. 3(4) (1999) 339-359.

[19] J. M. Sanches, J. S. Marques, A Rayleigh reconstruction/interpolation algorithm for 3D ultrasound, Pattern Recogn. Lett. 21(10) (2000) 917-926.

[20] R. W. Prager, A. H. Gee, L. Berman, Stradx: real-time acquisition and visualization of freehand three-dimensional ultrasound, Med. Image Anal. 3(2) (1999) 129-140.

[21] R. N. Rohling, A. H. Gee, L. Berman, Three-dimensional spatial compounding of ultrasound images, Med. Image Anal. 1(3) (1997) 177-193.

[22] C. Martinoli, S. Bianchi, M. Dahmane, F. Pugliese, M. P. Bianchi-Zamorani, M. Valle, Ultrasound of tendons and nerves, Eur. Radiol. 12(1) (2002) 44-55.

[23] P. R. Detmer, G. Bashein, T. Hodges, K. W. Beach, E. P. Filer, D. H. Burns, D. E. Strandness, 3D ultrasonic image feature localization based on magnetic scanhead tracking: in-vitro calibration and validation, Ultrasound Med. Biol. 20(9) (1994) 923-936.

[24] M. Levoy, Efficient ray tracing of volume data, ACM T. Graphic. 9(3) (1990) 245-261.

Figure Captions

Fig. 1. Coordinate systems in freehand 3D ultrasound imaging system with a position sensor.

Fig. 2. Diagram of the portable 3D free-hand ultrasound imaging system.

Fig. 3. The 3D translating device used for temporal calibration.

Fig. 4. Temporal calibration results. (a) The position data sets detected by the electromagnetic device and the ultrasound system at the sampling rate of 21 Hz, (b) the root-mean-square errors between the two data sets. The horizontal axis in (a) denotes the measurement time and that in (b) denotes the time delay between the two measurements.

Fig. 5. The construction of the volume coordinates system.

Fig. 6. Functions for defining ROI and scaling B-scans. (a) An original B-scan; (b) a scaled version of the B-scan, (c) a selected ROI of the B-scan, (d) the original B-scan with its position and orientation adjusted in real-time according to the recorded spatial information during image collection.

Fig. 7. A 2D representation of the volume reconstruction using a grid-mapping algorithm. For each voxel in the volume, a sphere region centred about it was defined. The distance from each pixel transformed into the region to the centre of the voxel was used to decide the weighted contribution of the pixel. The final value of the voxel was the weighted sum of the intensities of all pixels falling in this sphere region.

Fig. 8. Functions of volume analysis. (a) A clipped volume, (b) a display of three orthogonal slices of the finger volume.

Fig. 9. Reconstructed volumes of phantoms. (a) Cylinder phantom with its diameter and height indicated by the arrows, (b) cuboid phantom with its width, height, and length indicated by the arrows; (c) the right hand of the fetus phantom.

Fig. 10. Correlation between the dimensions measured using the micrometer and the 3D ultrasound system.

Fig. 11. Results of 3D ultrasound imaging for the subjects *in vivo*. (a) The volume of three fingers, (b) the volume of part of a forearm, (c) a typical slice obtained from the volume with the location and orientation indicated by the plane in (a), (d) the corresponding original B-scan image collected at the approximately same location of the slice showed in (c).

Fig. 12. Comparisons between the reconstruction results for a finger obtained using different interpolation algorithms. (a) A cross-sectional slice of the volume interpolated using DW method, (b) the same slice in the volume interpolated using the SDW method, (c) the same slice in the volume interpolated using the Gaussian convolution kernel method; (d), (e), (f) show the enlarged images for the portion marked on the slices of (a), (b), and (c), respectively. Results demonstrated that SDW method achieved improved image quality in comparison with DW method and reduced computation time in comparison with Gaussian kernel methods.

1

2

3

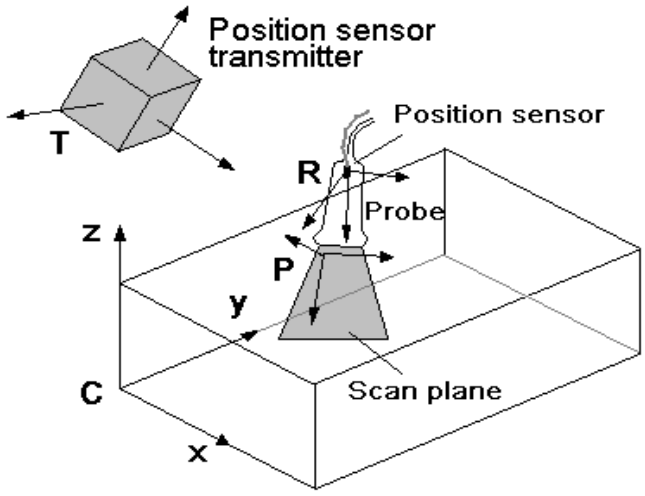
Position sensor
transmitter
T
Position sensor
R
Probe
z
P
y
C
Scan plane
x

Fig. 1

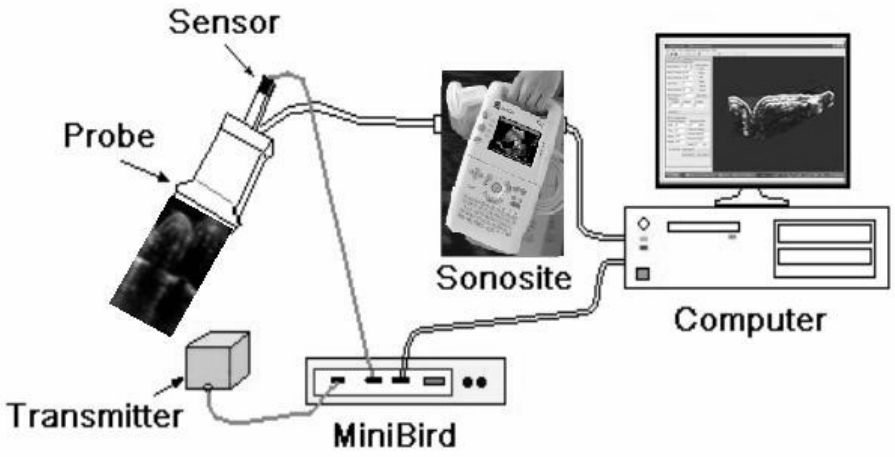
Sensor
Probe
Sonosite
Computer
Transmitter
MiniBird

Fig. 2

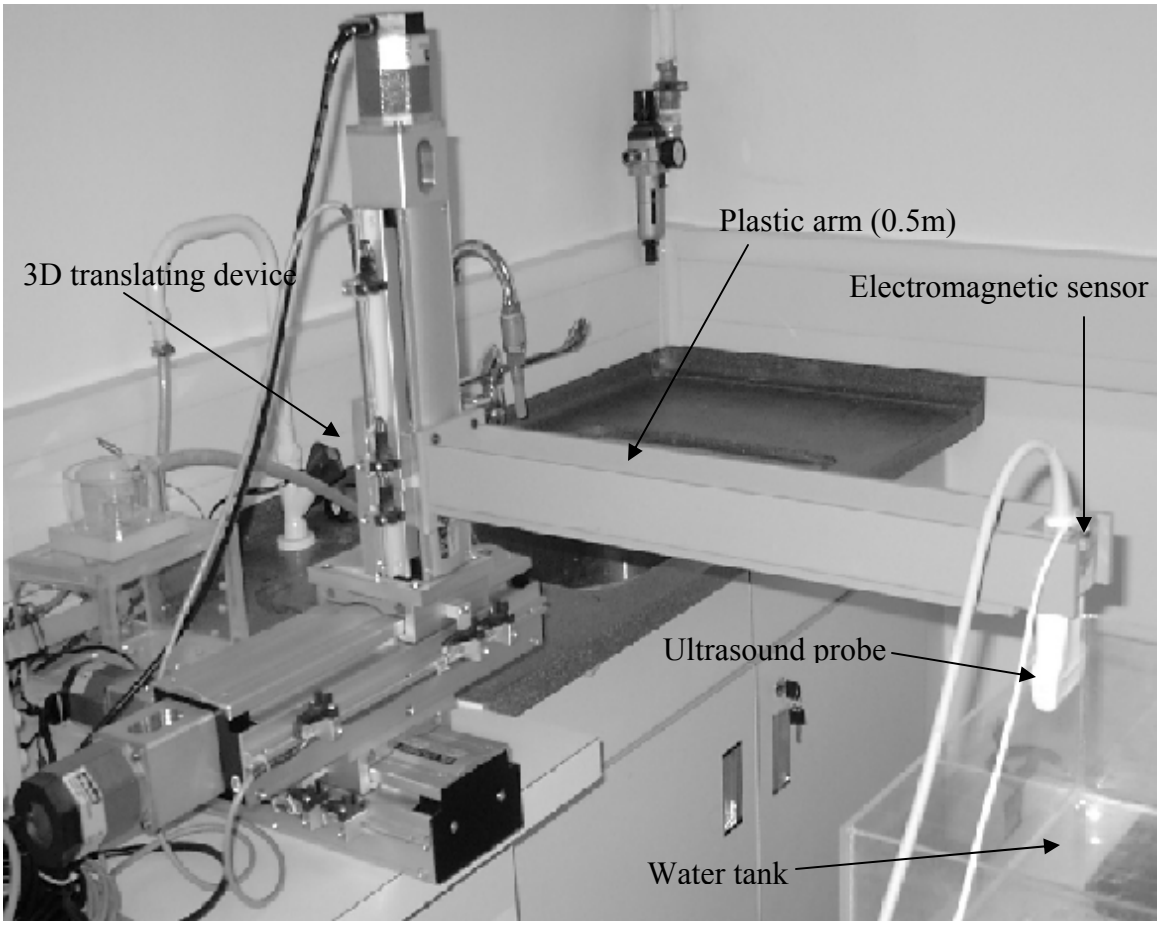
3D translating device
Plastic arm (0.5m)
Electromagnetic sensor
Ultrasound probe
Water tank

Fig. 3

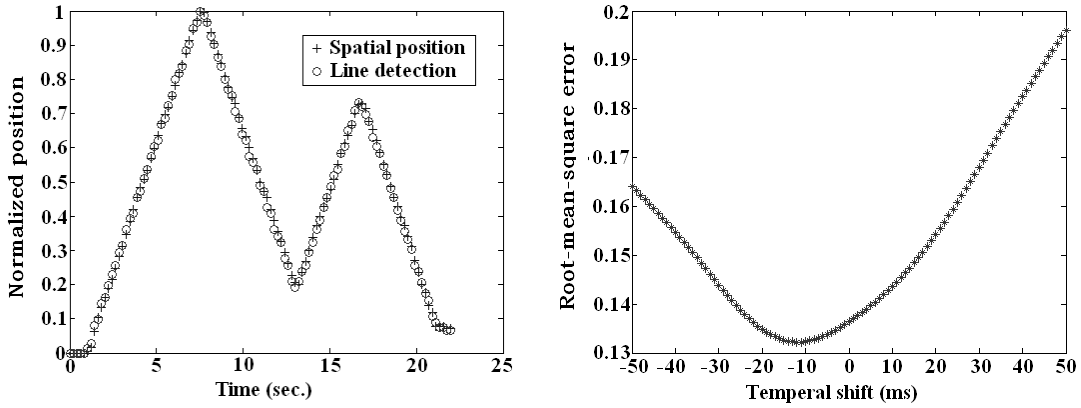
Normalized position
Time (sec.)
+ Spatial position
○ Line detection
Root-mean-square error
Temperal shift (ms)

(a) (b)

Fig. 4

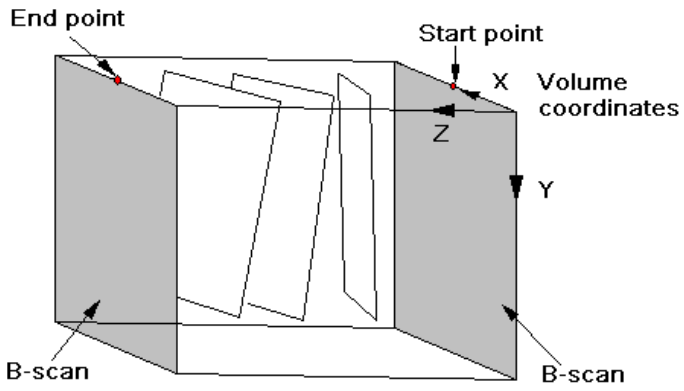

Fig. 5

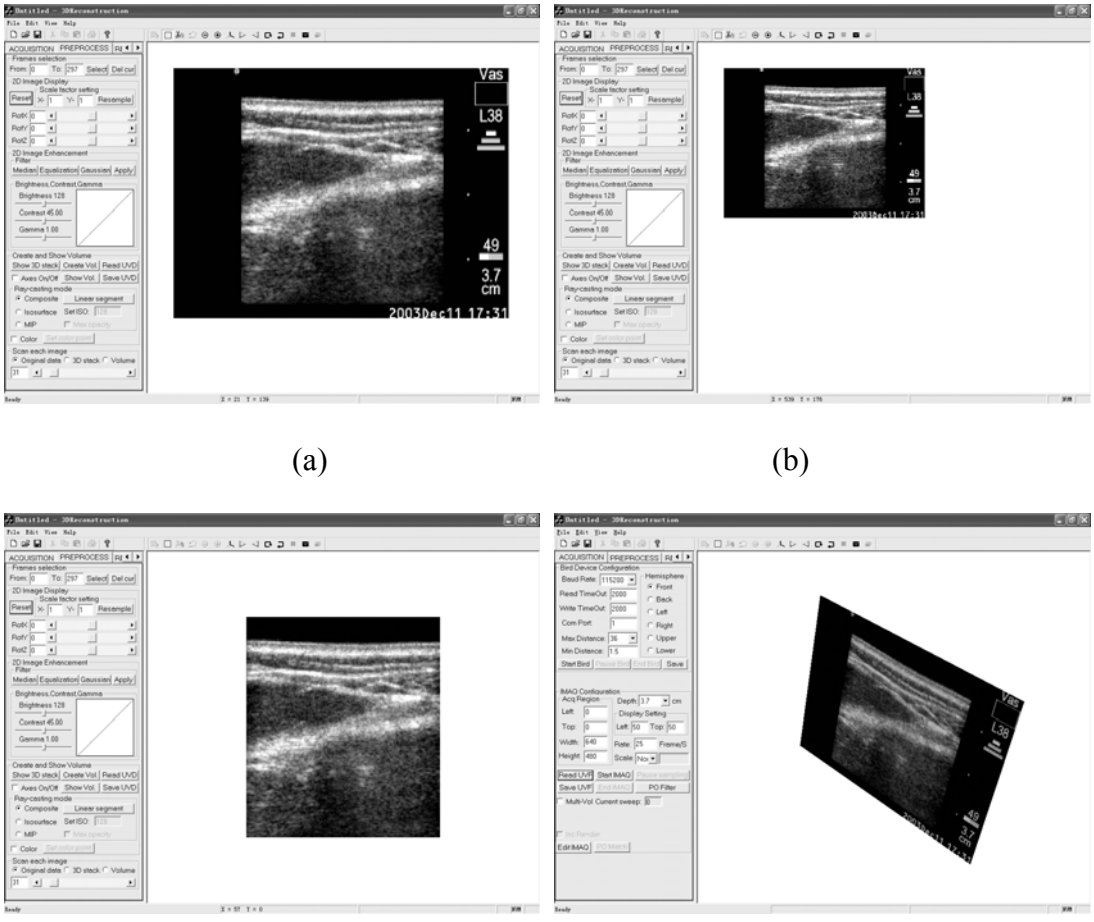

(a) (b)

(c) (d)

Fig. 6

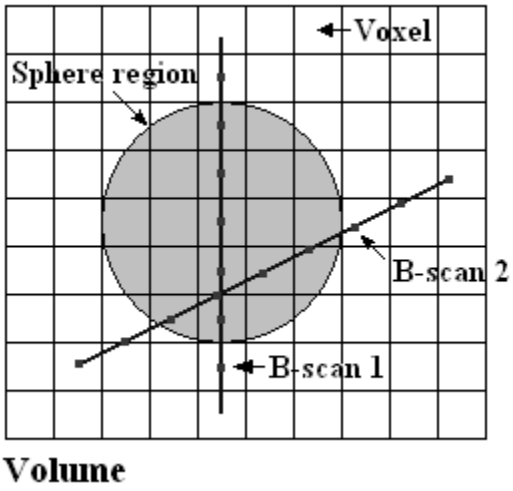
Voxel
Sphere region
B-scan 2
B-scan 1
Volume

Fig. 7

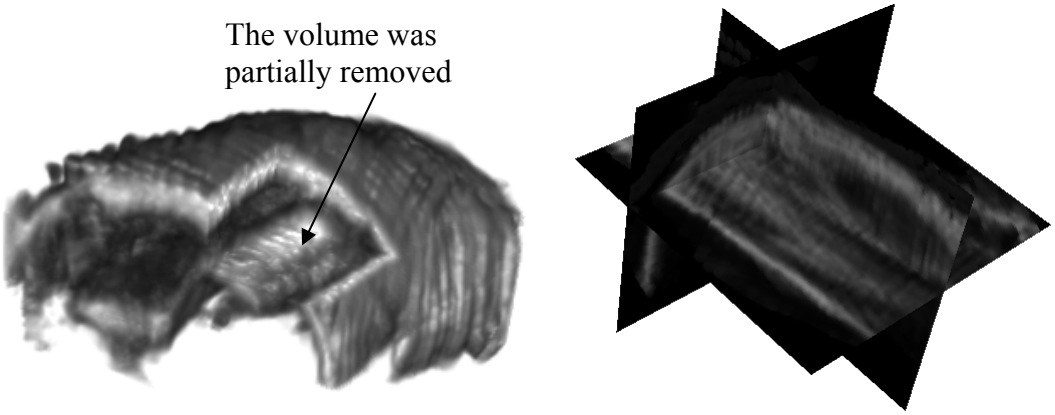
The volume was
partially removed

(a) (b)

Fig. 8

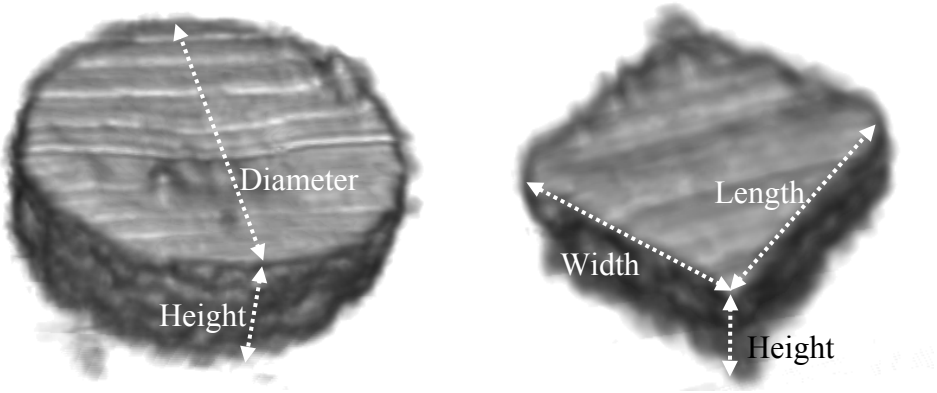
Diameter
Height
Length
Width
Height

(a) (b)

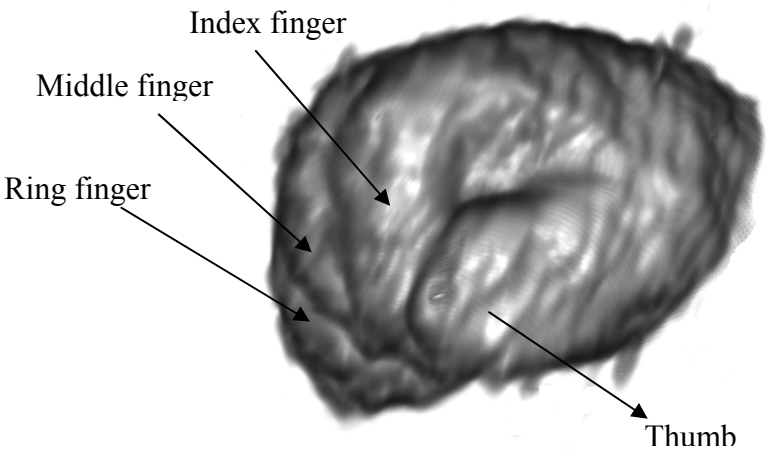
Index finger
Middle finger
Ring finger
Thumb

(c)

Fig. 9

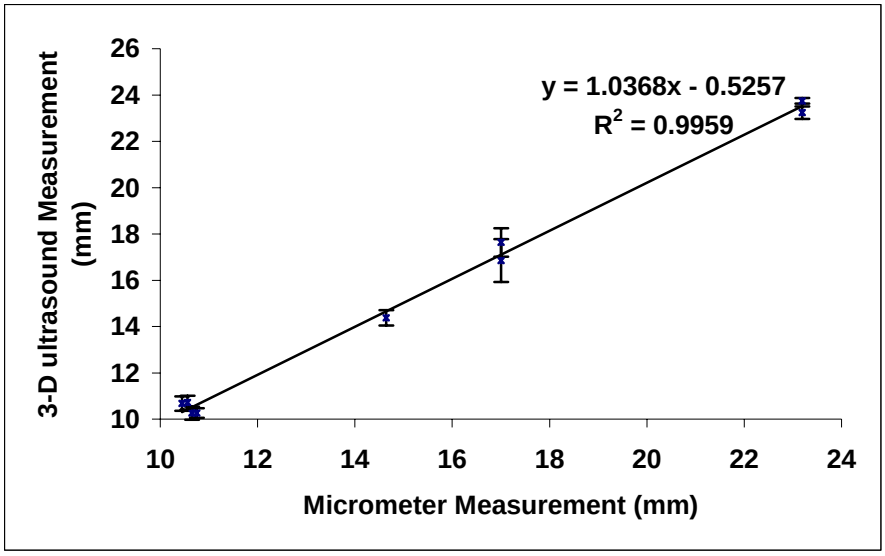
y = 1.0368x - 0.5257
R2 = 0.9959
3-D ultrasound Measurement (mm)
Micrometer Measurement (mm)
26
24
22
20
18
16
14
12
10
10
12
14
16
18
20
22
24

Fig. 10

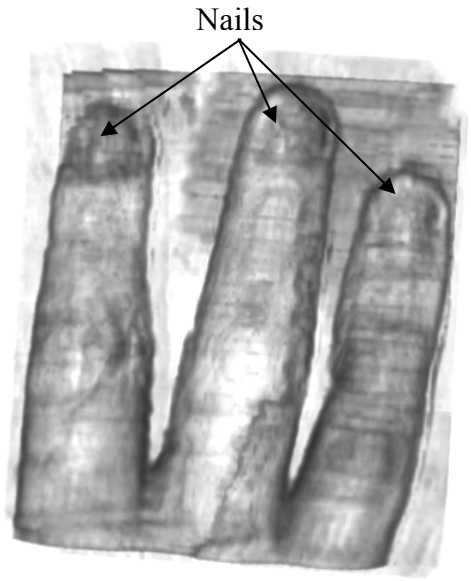
Nails

(a)

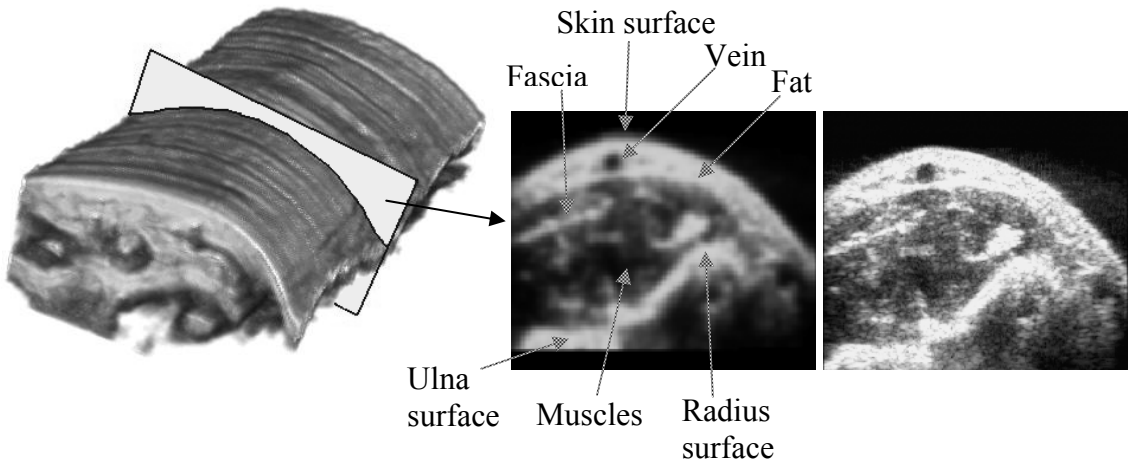

(b) (c) (d)

Fig. 11

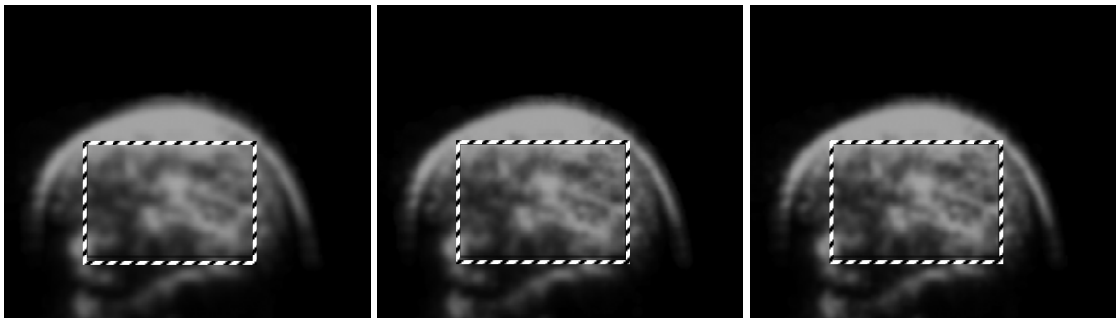

(a) (b) (c)

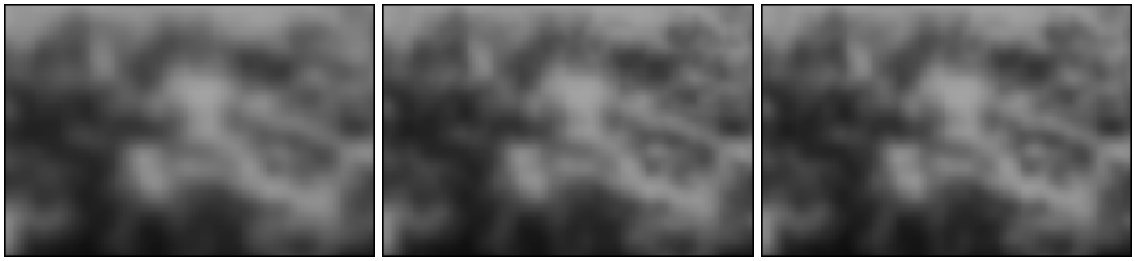

(d) (e) (f)

Fig. 12

Tables

Table 1. Results of the spatial calibration using the cross-wire phantom.

Table 2. Results of the validation experiments using the cylinder and cuboid phantoms.

Table 1

	Tx (mm)	Ty (mm)	Tz (mm)	α (radian)	β (radian)	γ (radian)
Mean	99.47	0.75	18.4	-1.558	0.083	-0.090
Variation with confidence level of 95%	1.62	0.60	0.84	0.037	0.038	0.074

Table 2

Phantom	Measurement items	Micrometer	Measurement from volume
Cylinder phantom	Diameter (mm)	23.19	23.75±0.12
	Height (mm)	10.75	10.26±0.21
	Volume (mm^3)	4540.5	4450.5±142.6
Cuboid phantom 1	Length (mm)	17.00	17.64±0.62
	Width (mm)	17.00	16.85±0.92
	Height (mm)	10.65	10.26±0.29
	Volume (mm^3)	3077.9	3046.5±179.4
Cuboid phantom 2	Length (mm)	10.56	10.72±0.30
	Width (mm)	10.45	10.67±0.32
	Height (mm)	14.64	14.37±0.33
	Volume (mm^3)	1615.6	1644.8±114.5